Shape-anisotropy-controlled magnetoresistive response in magnetic tunnel junctions

Yu Lu,[a] R. A. Altman, A. Marley,[b] S. A. Rishton, P. L. Trouilloud, Gang Xiao,[a]
W. J. Gallagher,[c] and S. S. P. Parkin[b]
IBM Research Division, T. J. Watson Research Center, Yorktown Heights, New York 10698

(Received 27 January 1997; accepted for publication 17 March 1997)

We show that shape anisotropy can be used to control the response characteristics of magnetic tunnel junctions. By varying the junction shape, the resistance versus field curve was made to vary from a nonhysteretic linear curve with a high-field sensitivity (0.3%/Oe) to a hysteretic response curve with high squareness. © *1997 American Institute of Physics.* [S0003-6951(97)04019-9]

Magnetoresistance (MR) in tunnel junctions with ferromagnetic metal electrodes on both sides was first demonstrated by Julliere[1] more than twenty years ago. Following two reports in 1995 of large (18%) MR effects at room temperature in magnetic tunnel junctions (MTJs),[2,3] there has been renewed interest in these devices.[4] For instance, we recently showed that deep submicron MTJs can be made with large MRs (>20%) and reasonable resistance levels.[5,6] In this letter, we demonstrate control of the magnetic response through shape anisotropy and discuss the magnetic coupling between the electrode layers.

The magnetoresistance effect in tunnel junctions with nonmagnetic barriers arises from the spin imbalance in the electron density of states (DOS) in ferromagnetic metals. In the absence of spin–flip scattering, the tunneling current can be separated into spin up and spin down currents, defined with respect to the magnetization direction of one of the electrodes (assuming, for ease of discussion, uniformly magnetized electrodes). When the magnetic moments of the electrodes are aligned parallel to each other, there is an optimum match of filled majority spin states in one electrode with empty majority spin states in the other electrode, and the net tunneling current is a maximum. When the moments are antiparallel to each other, a DOS mismatch of spin up and spin down components results in a minimum of total tunneling current. Slonczewski[7] showed that tunneling conductance is proportional to the cosine of the angle between the magnetic moment vectors in the two electrodes. Of course, actual MTJ devices will not, in general, have electrodes that are uniformly magnetized and their magnetoresistive response will be complicated by the detailed magnetic reversal processes within the electrodes.

Microlithographic techniques are required to fabricate small devices of accurately defined shape and size. Details of our fabrication process have been described elsewhere.[5,6] In what follows, we briefly review the procedure for making the devices used here. First, a multilayered film containing the junction structure is sputter deposited onto a Si wafer. For the devices used in this work, in particular, the layer sequence is Si(100)/50Ta/200Pt/40Py/100FeMn/60Py/20Co/Al–O/150Py/200Ta, where the numbers are layer thickness in angstroms and Py refers to permalloy $Ni_{81}Fe_{19}$. The 40Py layer, the 60Py/20Co bilayer, and the 150Py layer are referred to as the seed layer, pinned layer (bottom electrode), and free layer (top electrode), respectively. The bottom junction electrode is pinned by exchange bias from the 100FeMn layer. The purpose of the Co in the bilayer used for the pinned layer is to increase the spin polarization at the barrier interface. The aluminum oxide (Al–O) barrier layer was formed by depositing 9.5 angstroms of Al and then plasma oxidizing it for 30 s. A magnetic field of about 100 Oe is applied in the plane of the film during deposition to induce a uniaxial anisotropy, and thereby, define the exchange pinning direction and the easy-axis direction of the free layer. The magnetic properties of blanket film multilayer structures are characterized using a vibrating sample magnetometer (VSM).

A self-aligned lithographic process is used to pattern the device structures.[4,5] For the devices reported here, optical lithography was used with a minimum feature size of about 1 μm. First, the base electrode and the junction top electrode area are defined by a sequence of two ion milling processes. The second milling step is timed to stop just below the top surface of the bottom electrode, some overmilling being inevitable. This overmilling has important effects on the magnetic coupling of the two electrodes. Next, the junctions are coated with a SiO_2 insulating layer, which is lifted off to expose self-aligned contact holes to the junction top electrode. Finally, contact pads and wiring to the top electrode are patterned out of a subsequent metallization layer. Figure 1 shows schematic drawings of the finished junction structure (a) in a cross-sectional view and (b) in a top view showing some typical junction shapes (b). Our mask patterns include 200 junctions on a quarter of a 1 in. silicon wafer with various junction areas ($1-10^4$ μm^2) and shapes (mostly rectangular).

The MTJ devices on the chip are measured electrically using a probe station in ambient environment. A magnetic field along the easy axis of the film is applied to change the magnetic states of the devices. The field uniformity is better than 1% over the area of the chip. The dynamic tunneling resistance (dV/dI) is measured using an ac method with zero dc bias. Voltage amplitude on the junction is kept smaller than 10 $mV_{p\text{-}p}$ to avoid the voltage dependent degradation of the MR effect.[1,3]

Figure 2(a) shows the magnetization $\boldsymbol{M}$ hysteresis curve of the sheet multilayer film (one quarter of a 1 in. diam wafer) measured using the VSM. There are three well-

[a]Also at: Physics Department, Brown University, Providence, RI 02912.
[b]IBM Research Division, Almaden Research Center, Almaden, CA 95120.
[c]Electronic mail: glgr@watson.ibm.com

Downloaded¬11¬Jul¬2001¬to¬128.148.60.155.¬Redistribution¬subject¬to¬AIP¬license¬or¬copyright,¬see¬http://ojps.aip.org/aplo/aplcr.jsp

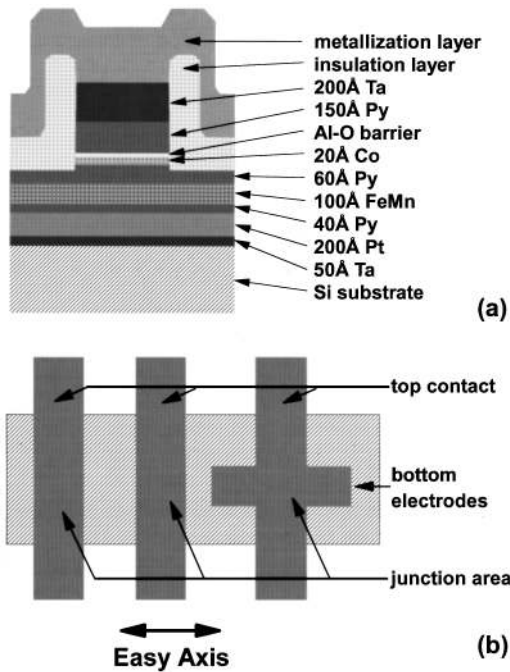

FIG. 1. Schematic drawing showing MTJ device structure: (a) cross-sectional view, and (b) top view of typical device geometries.

separated subloops corresponding to the magnetic reversal of the seed layer, the pinned layer, and the free layer, in order of increasing net magnetizations (due to the layers' different thicknesses). Figure 2(b) shows the tunneling resistance of a 2.5 μm$\times$12.5 μm device as a function of the magnetic field applied along the easy axis of the film, which is also the long axis of the junction. The two hysteresis loops seen in Fig. 2(b) are due to the corresponding loops of the pinned layer

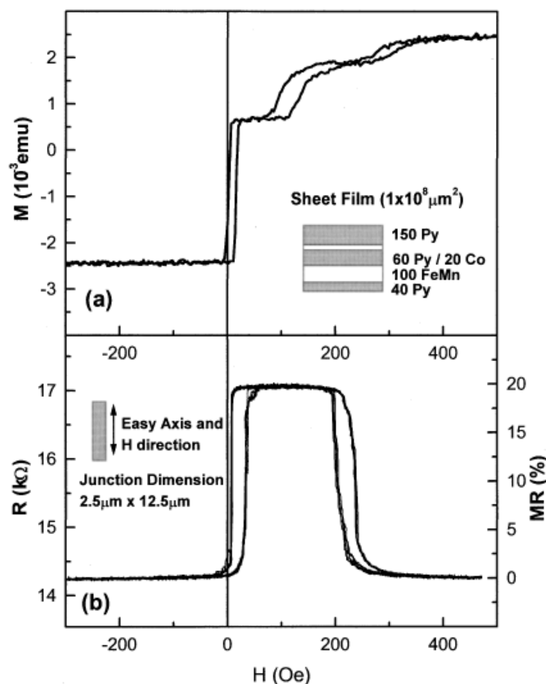

FIG. 2. (a) Magnetic hysteresis loop of sheet film with multilayer junction structures. (b) Tunneling resistance R and magnetoresistance ratio $\Delta R/R_p$, vs magnetic field along the easy axis of a MTJ with a rectangular 2.5$\times$12.5 μm^2 top electrode.

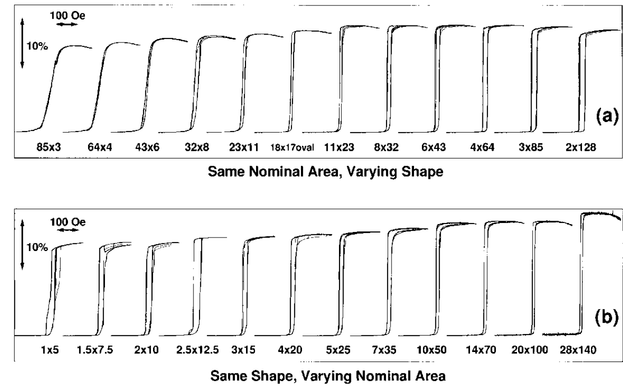

FIG. 3. (a) Junction resistance versus magnetic field for series A devices, which have the same nominal junction area but different shapes. The first number in the label is the dimension of the junction top electrode along the hard axis in μm, while the second number is the dimension along the easy axis. (b) Junction resistance versus magnetic field for series B devices, with different areas but the same nominal 1–5 aspect ratio for the junction top electrode. The unusually large MR in the largest junction 28$\times$140 (μm^2) is due to a nonuniform current distribution effect as discussed in Ref. 8.

and the free layer. The exchange bias shown in the tunneling resistance data is much stronger than that of the sheet film. This can be explained by the reduced pinned-layer thickness due to overmilling in the area surrounding the junction, which acts to stabilize the magnetization of the junction base electrode (which is not reduced in thickness).

The size of the MR effect can be understood within the simple model proposed by Julliere.[1] The MR ratio for the devices described above should be given by

$$\Delta R/R_p=(R_{ap}-R_p)/R_p=2P_{Co}P_{Py}/(1-P_{Co}P_{Py}), \qquad (1)$$

where R_p and R_{ap} are the resistances for the parallel and antiparallel $\boldsymbol{M}$ configurations, respectively, and P_{Co} and P_{Py} are the spin polarization of the Co ($P_{Co}\approx 0.35$) and Py ($P_{Py}\approx 0.30$) electrodes.[9] For our MTJ devices, we expect MR$=\Delta R/R_p=24.5\%$, which is in agreement with the values we observe. This is consistent with tunneling being the main conduction mechanism and with the barrier being free of magnetic impurities and other spin–flip scattering centers.

Figures 3(a) and 3(b) show the resistance versus magnetic-field curves of two series (hereafter, called series A and B, respectively) of devices on the chip, normalized to their saturation resistance R_p. The magnetic-field sweep range is limited so that only the free-layer magnetization reverses. Devices in series A all have the same normal area, but the shape of the rectangle is evolving from a needlelike rectangle perpendicular to the easy axis of the film (which is also the magnetic-field direction) at the left end of the plot to a squarish shape in the middle of the series to a thin needle along the easy axis at the right end. Devices in series B have varying size but the same shape, in this case, rectangles with a 5:1 aspect ratio along the easy-axis direction.

The changing response characteristic of the curves in Fig. 3(a) demonstrates that the shape anisotropy in our devices is more important than the intrinsic anisotropy induced during film deposition. Thus, the MR response of the MTJ devices can be ''engineered'' by simply changing the shape of the free-layer electrode. At the left end of the plot where

Downloaded¬11¬Jul¬2001¬to¬128.148.60.155.¬Redistribution¬subject¬to¬AIP¬license¬or¬copyright,¬see¬http://ojps.aip.org/aplo/aplcr.jsp

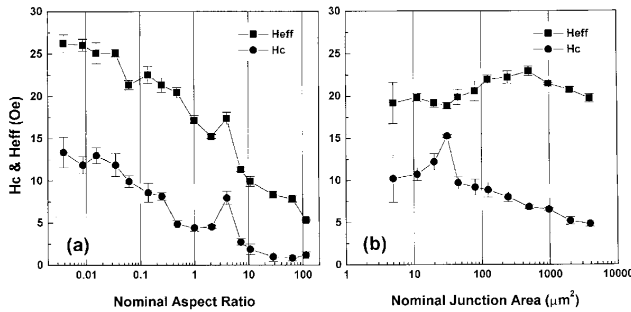

FIG. 4. (a) Coercive force H_c and effective coupling field $H_{\rm eff}$ as a function of the nominal junction aspect ratio for series A devices. The error bar indicates the variation of these quantities with multiple cycles of the magnetic field. (b) H_c and $H_{\rm eff}$ as a function of the junction area for series B devices, which all have a 1–5 nominal aspect ratio.

the electrodes are shaped as thin rectangles normal to the easy axis, the demagnetization field will break the magnetization into a buckled domain pattern. The magnetic reversal, in this case, will most likely be a combination of rotation and domain-wall motion. The MR curve reflects the averaged responses of these domains and is linear and nearly nonhysteretic. The field sensitivity reaches up to 0.3%/Oe (in the 64×4 $\mu\mathrm{m}^2$ junction). At the right end of Fig. 3(a), it is most likely that reversal domains nucleate at the ends and/or around edge roughness, and sweep through the whole device when the domain pinning force is exceeded, giving rise to a square hysteresis loop with discontinuous jumps in resistance. In Kerr images taken of some of our devices, we have seen evidence for this reversal mechanism. Figure 3(b) shows, however, that this simple picture gets more complicated with junction areas below 100 $\mu\mathrm{m}^2$. In this case, we believe edge roughness and other defects play an increasingly important role.

Figures 4(a) and 4(b) show the coercive force H_c and the effective coupling field $H_{\rm eff}$ (center of the hysteresis loops) in series A and B, as a function of aspect ratio (hard-axis-side length to easy-axis-side length) and nominal junction area, respectively. The coercive force drops with increasing aspect ratio, as expected from the increased demagnetization factor, although the dependence is weaker than simple expectations from a single-domain picture. The slight drop in H_c with larger junction size can possibly be explained by the increased probability of finding a nucleation site with smaller coercive force in the top electrode.

The effective coupling field has two dominant sources: Néel ''orange-peel'' coupling (ferromagnetic) due to correlated interface roughness[10] and stray field coupling (antiferromagnetic) due to poles in the overmilled pinned layer. The Néel coupling depends only on the sheet film parameters (free-layer thickness, barrier thickness, and roughness) and should be independent of device geometry. The stray field coupling depends on the amount of overmilling as well as the actual shape of the junction electrodes, and increases with decreasing length along the easy-axis direction. The sum of these two effects determines the overall coupling strength, which is reflected in the quantity $H_{\rm eff}$. The data in Figs. 4(a) and 4(b) show that $H_{\rm eff}$ is ferromagnetic. The size of $H_{\rm eff}$ increases significantly with decreasing aspect ratio, reflecting the strong shape dependence of the stray field coupling. For fixed aspect ratio, Fig. 4(b) shows that there is not a strong size dependence of $H_{\rm eff}$, indicating that the stray field coupling is not strongly size dependent over the range of sizes studied.

The above discussion neglects exchange coupling through the barrier. Compared to spin valves with metallic spacer layers, the exchange coupling in tunnel junctions should be smaller due to the insulating nature of the tunnel barrier, less than 10^{-3} Oe according to a estimate made following Ref. 7. On the other hand, the extreme thinness of the oxide tunnel barrier leads to larger Néel orange peel coupling.

In conclusion, we have demonstrated that the magnetoresistance effect in magnetic tunnel junctions can be controlled by the shape anisotropy of the top electrode. Linear responses with high-field sensitivity (0.3%/Oe) and hysteretic responses with high squareness can be achieved on the same chip. In all cases, the size of the MR effect at room temperature is consistent with estimates made using Julliere's spin-polarized tunneling model. The magnetic coupling between the electrodes in the tunnel junction is dominated by a combination of orange-peel coupling and stray magnetostatic field coupling.

The authors wish to thank J. C. Slonczewski, X. W. Li, K. P. Roche, S. L. Brown, J. J. Connolly, A. Gupta, G. Q. Gong, and R. Laibowitz for stimulating discussions and help. The work at Brown University was partially supported by National Science Foundation Grant Nos. DMR-9414160 and DMR-9258306 and at IBM partially by DARPA and by the Office of Naval Research.

[1] M. Julliere, Phys. Lett. A **54A**, 225 (1975).
[2] T. Miyazaki and N. Tezuka, J. Magn. Magn. Mater. **139**, L231 (1995).
[3] J. S. Moodera, L. R. Kinder, T. M. Wong, and R. Meservey, Phys. Rev. Lett. **74**, 3273 (1995).
[4] J. S. Moodera and L. R. Kinder, J. Appl. Phys. **79**, 4724 (1996); C. L. Platt, B. Dieney, and A. E. Berkowitz, Appl. Phys. Lett. **69**, 2291 (1996); K. Matsuyama, H. Asada, H. Miyoshi, and K. Taniguchi, IEEE Trans. Magn. **31**, 3176 (1995); Yu Lu, X. W. Li, G. Q. Gong, A. Gupta, P. Lecoeur, J. Z. Sun, Y. Y. Wang, and V. P. Dravid, Phys. Rev. B **54**, 8357 (1996); J. Z. Sun, W. J. Gallagher, P. R. Duncombe, L. Krusin-Elbaum, R. A. Altman, A. Gupta, Yu Lu, G. Q. Gong, and G. Xiao, Appl. Phys. Lett. **69**, 3266 (1996).
[5] W. J. Gallagher, S. S. P. Parkin, Yu Lu, X. P. Bian, A. Marley, R. A. Altman, S. A. Rishton, K. P. Roche, C. Jahnes, T. M. Shaw, and G. Xiao, J. Appl. Phys. (in press).
[6] S. Rishton, Y. Lu, R. A. Altman, A. C. Marley, X. P. Bian, C. Jahnes, G. Xiao, W. J. Gallagher, and S. S. P. Parkin, Magnetic Tunnel Junctions Fabricated at Tenth-Micron Dimensions by Electron Beam Lithography, Microelectronic Engineering Conference Proceedings, 1996 (in press).
[7] J. C. Slonczewski, IBM Tech. Discl. Bull. **19**, 2328 (1976); J. C. Slonczewski, Phys. Rev. B **39**, 6995 (1989).
[8] J. S. Moodera, L. R. Kinder, J. Nowak, P. LeClair, and R. Meservey, Appl. Phys. Lett. **69**, 708 (1996).
[9] For a review of spin-polarized tunneling studies, see, e.g., R. Meservey and P. M. Tedrow, Phys. Rep. **239**, 174 (1994).
[10] L. Néel, C. R. Acad. Sci. **255**, 1676 (1962).

Downloaded¬11¬Jul¬2001¬to¬128.148.60.155.¬Redistribution¬subject¬to¬AIP¬license¬or¬copyright,¬see¬http://ojps.aip.org/aplo/aplcr.jsp